Complex third-order nonlinear susceptibility of single-layer graphene governing third-harmonic generation

Daiki Inukai,[1] Takeshi Koyama,[1] Kenji Kawahara,[2] Hiroki Ago,[2] and Hideo Kishida[1,*]
[1]*Department of Applied Physics, Nagoya University, Nagoya, Aichi 464-8603, Japan*
[2]*Global Innovation Center (GIC), Kyushu University, Kasuga, Fukuoka 816-8580, Japan*

(Received 28 March 2023; accepted 28 June 2023; published 11 August 2023)

The resonant process of the third-order nonlinear optical response of single-layer graphene has been investigated using various approaches. The complex third-order nonlinear susceptibility ($\chi^{(3)}$) directly reflects the resonance effects in third-order nonlinear processes. We measured the modulus and phase of $\chi^{(3)}$ governing the third-harmonic generation (THG) of graphene using the Maker fringe method. First, we observed the incident photon energy dependence of THG in the energy range from 0.57 to 0.81 eV. The modulus values of $\chi^{(3)}$ decreased from 7×10^{-10} to 2×10^{-10} esu, with an increase in photon energy. The phase values increased from 330° to 360° in the corresponding energy range. When the experimental result and the model calculation were compared, we found that the THG process in graphene can be described by the superposition of one-, two-, and three-photon resonant components. Experimental results demonstrate that the two-photon resonant process comprising interband and intraband transitions is the most significant among the three components for THG in graphene. Second, we measured the Fermi energy (E_F) dependence of THG in the range of -568 meV $\leqslant E_F \leqslant +133$ meV at incident photon energies of 0.60 and 0.72 eV. The modulus of $\chi^{(3)}$ changed from 5.4×10^{-11} to 6.4×10^{-10} esu with doping. This result is due to the reduction of the one-photon resonant component by Pauli blocking. The complex $\chi^{(3)}$ has positive real and negative imaginary parts regardless of E_F. We also analyzed the laser power dependence of THG intensity via model calculation taking account of the electron temperature. The experimental results and discussion of the complex $\chi^{(3)}$ of graphene can be a basis for understanding nonperturbative harmonic generation and other third-order nonlinear optical responses in Dirac materials.

DOI: 10.1103/PhysRevB.108.075408

I. INTRODUCTION

Nonlinear optical (NLO) spectroscopy clarifies electronic processes under strong electric fields. In the regime of moderately strong fields, NLO processes can be understood using perturbation theory. NLO spectroscopy unravels the excited-state structures of various electronic systems [1–5]. Particularly, third-order nonlinear spectroscopy has been successful at revealing the electronic structures of low-dimensional systems [5–8]. Recently, NLO spectroscopic studies have been extended to the high electric field regime. Higher-harmonic generation has been researched intensively [9,10] and applied to low-dimensional materials [11] and Dirac electronic systems [12,13]. In these studies, information on detailed electronic structures is important in achieving a grounded understanding of the nonperturbative regime. For example, in the high electric field regime, the *i*th high-harmonic generation is not proportional to the *i*th power of incident light, where the mixing of multiple orders of perturbations plays a key role. To understand such high-order and nonperturbative optical processes, information regarding electronic structures revealed by the lowest-order perturbative NLO process, namely, the third-order NLO process, can be crucial.

Several experimental results on third-harmonic generation (THG) in single-layer graphene have been reported at various excitation photon energies ($\hbar\omega$) [14–20]. The moduli of complex third-order nonlinear susceptibility, denoted as $|\chi^{(3)}|$, in previous reports vary by as much as five orders of magnitude [14–20]. This discrepancy has two possible reasons. The first one is the $\hbar\omega$ dependence of the resonance effect [19]. The resonant structure in the $\chi^{(3)}$ spectra is affected by the governing electronic states, transition matrix elements, and density of states. Previous experimental research has revealed a broadband THG spectrum, which reflects the linear band dispersion of graphene, and the THG intensity (I_{THG}) is enhanced by 100 times as the incident photon energy changes from 0.7 to 0.4 eV [19]. The second one is that $\chi^{(3)}$ depends strongly on the Fermi energy (E_F), defined as the energy from the Dirac point. A nonzero E_F prohibits electronic transitions whose energy is lower than $2|E_F|$ because the conduction (valence) band is filled with electrons (holes) up to E_F. Therefore, a nonzero E_F influences the resonance mechanism in the THG process, and the value of $|\chi^{(3)}|$ exhibits a strong E_F dependence [18–21]. In fact, Jiang *et al.* reported a tenfold enhancement of $|\chi^{(3)}|$ based on electrochemical doping that shifts E_F from 0 to -0.89 eV [18]. Additionally, we should focus on the experimental fact that the exponent of incident laser power (I_ω) dependence of THG deviates from 3 according to E_F [20]. In the report, the laser power dependence is explained by the rise of electron temperature (T_e) due to

*kishida@nagoya-u.jp

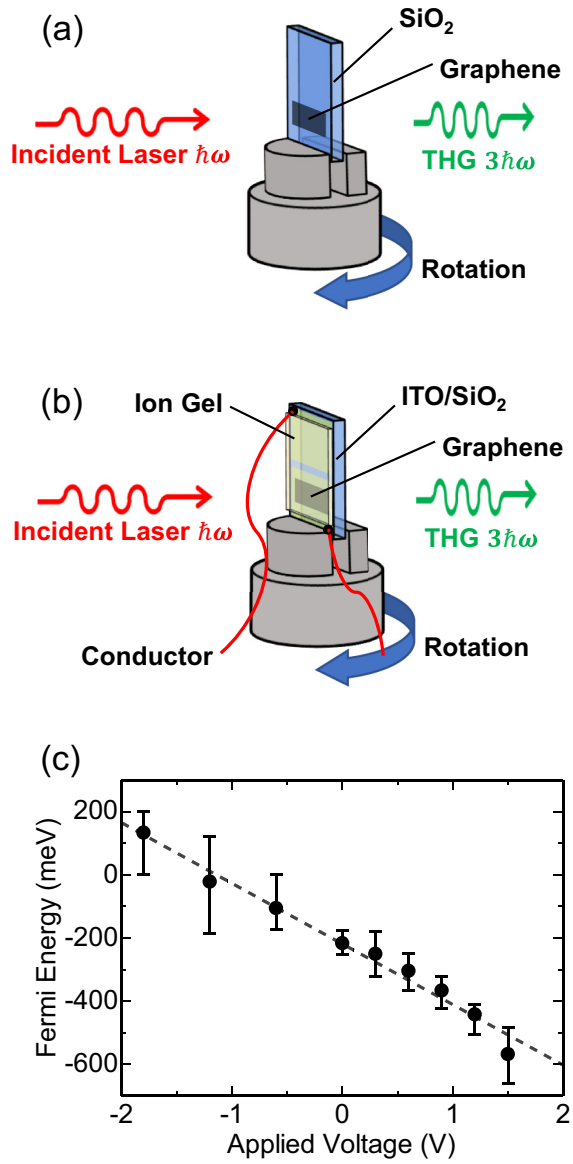

FIG. 1. Schematic illustration of the Maker fringe method (a) for as-grown single-layer graphene on the SiO_2 substrate and (b) for the electrochemical doping device of graphene using an ion gel. (c) Applied voltage dependence of the Fermi energy E_F of graphene on the electrochemical doping device. The broken line is an approximate straight line.

one-photon absorption of the incident laser pulse [18–20]. As the absorption coefficient at $\hbar\omega$ and the specific heat of the electron depend on E_F, T_e varies with E_F for the same incident laser power. In a previous study, the power law of $I_{\mathrm{THG}} \propto I_\omega^3$ collapsed, and the exponent varied from 2.2 to 3.3 according to E_F [20]. Thus, even within the perturbative third-order NLO response of graphene, laser power dependence can be significantly deviated from $I_{\mathrm{THG}} \propto I_\omega^3$ depending on the incident photon energy, Fermi energy, and incident laser power.

Although Jiang *et al.* observed a high degree of consistency between their experimental results for $|\chi^{(3)}|$ [18] and calculation results [21], they did not discuss $\chi^{(3)}$ as a

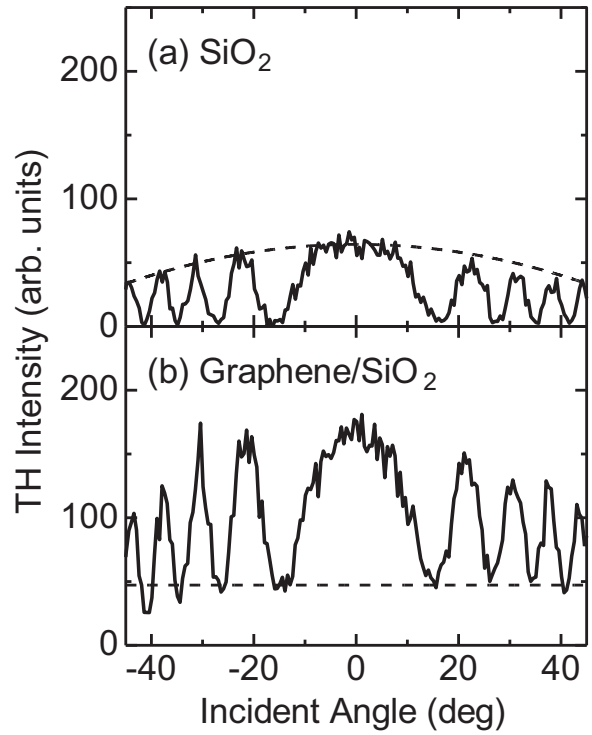

FIG. 2. Intensity pattern of TH as a function of the incident angle (a) for a SiO_2 substrate (1 mm thick) and (b) as-grown single-layer graphene on a SiO_2 substrate at an excitation wavelength of 2066 nm (0.60 eV). Solid lines represent the experimental results. Broken lines in (a,b) represent the TH intensities of $I_{3\omega,\mathrm{S}}$ and $I_{3\omega,\mathrm{G}}$, respectively.

complex quantity, which more directly reflects resonance. The energy denominators of $\chi^{(3)}$, namely, $[E-m\hbar\omega-i\Gamma]^{-1}$ ($m = 1,\ 2,$ and 3), are purely imaginary at resonance [1,2,4,6]. Here, E and Γ are the energy and damping energy of the excitation level, respectively. Therefore, the phase values should be close to $\pi/2$ or $3\pi/2$. However, the energy denominators are approximately purely real in a nonresonant condition, indicating that the phase values are close to zero or π. Therefore, the clarification of $\chi^{(3)}$ enables us to directly understand the resonance effects in THG. Actually, the complex $\chi^{(3)}$ spectra were experimentally measured for thin films of π and σ conjugated polymers [4,6]. The two resonant structures are observed in the $|\chi^{(3)}|$ spectra of polysilanes. The structures were attributed to the three- and two-photon resonance from the phase spectrum [6]. Accordingly, $\chi^{(3)}$ was desired to be measured for graphene also, and we measured $\chi^{(3)}$ to reveal the dominant electronic processes related to THG in graphene in this study.

II. EXPERIMENTAL METHOD

Single-layer graphene films were grown on Cu(111)/sapphire substrates via chemical vapor deposition [22] and then transferred onto substrates by a standard wet transfer technique using a polymethyl methacrylate support layer. A third-harmonic (TH) signal of single-layer graphene was observed using the Maker fringe method [23]. In this experiment, seed pulses from a mode-locked Ti-sapphire laser (800 nm, 80 MHz) were amplified using a regenerative

amplifier (1 kHz, 800 nm, and 100 fs). The wavelength of the amplified pulse was converted to 1530–2479 nm (0.57–0.81 eV) using an optical parametric amplifier (OPA). Laser pulses from the OPA were focused onto a sample placed in a vacuum chamber. The TH signal (510–826 nm) generated from the sample was extracted using a monochromator and detected using a photomultiplier. We obtained the fringe pattern of the TH light by measuring the intensity of the THG while varying the optical length by rotating the sample.

In the $\hbar\omega$ dependence experiment, we used as-grown graphene on a SiO_2 substrate (graphene/SiO_2, thickness $d_S = 1$ mm) shown in Fig. 1(a). Here, E_F of the as-grown graphene was determined to be -250 meV by Raman spectroscopy (see Supplemental Material, S1 [24]). In the E_F dependence experiment, we prepared an electrochemical doping device using an ion gel [25]. Figure 1(b) shows the structure of the doping device. In the device, indium tin oxide (ITO)/SiO_2 glass (11 mm × 15 mm) was used as a substrate. Here, the thicknesses of SiO_2, d_S, and ITO, d_I, are 1 mm and 120 Å, respectively. ITO works as a transparent electrode, and we prepared two ITO electrodes on one SiO_2 substrate. Graphene was transferred on one side of the ITO electrodes. To prepare an ion gel, we mixed 0.55 g of an ionic liquid, 1-ethyl-3-methylimidazolium bis(trifluoromethylsulfonyl)imide [(EMIM)(TFSI)], 21 mg of polystyrene-*b*-poly(ethylene oxide)-*b*-polystyrene (PS-PEO-PS) triblock copolymer (10–44–10 kg/mol), and 2 ml of dry dichloromethane under N_2 atmosphere at 300 K [26]. Here, (EMIM)(TFSI) was degassed in advance, and mixing was performed by stirring at 300 rpm for 12 h. The ion gel was spin coated onto the graphene/ITO/ SiO_2 substrate at a rate of 4000 rpm. By applying voltage V_a between two the ITO electrodes, E_F was shifted, as shown in Fig. 1(c). E_F was determined by the peak wave number of G and 2D phonons in the Raman spectrum [27,28] (see Supplemental Material, Fig. S1 [24]) and was controlled up to -568 meV. Analysis was conducted with reference to our previous research [25]. In our Raman scattering measurements, we used a He-Ne laser (632.8 nm) as an excitation light source, a 50× objective lens (spot diameter: 2 μm), and a diffraction grating of 1800 l/mm (wave number resolution: 0.9 cm^{-1}).

III. MODEL CALCULATION

In graphene, as the electronic states are not discrete but continuous, the electronic processes between numerous electronic states should be considered. The experimentally observed THG results are due to the superposition of multiple THG processes. The $\chi^{(3)}$ corresponding to THG is described by the following equation [1]:

$$\begin{aligned}\chi^{(3)}(\hbar\omega,\, E_F,\, T_e) \propto \int & f_0[E_0(\boldsymbol{q}),\, E_F,\, T_e]\{1 - f_0[-E_0(\boldsymbol{q}),\, E_F T_e,\,]\} \\ & \times \left[\frac{\langle 0,\boldsymbol{q}|r|3,\boldsymbol{q}\rangle\langle 3,\boldsymbol{q}|r|2,\boldsymbol{q}\rangle\langle 2,\boldsymbol{q}|r|1,\boldsymbol{q}\rangle\langle 1,\boldsymbol{q}|r|0,\boldsymbol{q}\rangle}{[E_{3,0}(\boldsymbol{q}) - 3\hbar\omega - i\gamma_{3,0}][E_{2,0}(\boldsymbol{q}) - 2\hbar\omega - i\gamma_{2,0}][E_{1,0}(\boldsymbol{q}) - \hbar\omega - i\gamma_{1,0}]} \right. \\ & + \frac{\langle 0,\boldsymbol{q}|r|3,\boldsymbol{q}\rangle\langle 3,\boldsymbol{q}|r|2,\boldsymbol{q}\rangle\langle 2,\boldsymbol{q}|r|1,\boldsymbol{q}\rangle\langle 1,\boldsymbol{q}|r|0,\boldsymbol{q}\rangle}{[E_{3,0}(\boldsymbol{q}) + \hbar\omega - i\gamma_{3,0}][E_{2,0}(\boldsymbol{q}) - 2\hbar\omega - i\gamma_{2,0}][E_{1,0}(\boldsymbol{q}) - \hbar\omega - i\gamma_{1,0}]} \\ & + \frac{\langle 0,\boldsymbol{q}|r|3,\boldsymbol{q}\rangle\langle 3,\boldsymbol{q}|r|2,\boldsymbol{q}\rangle\langle 2,\boldsymbol{q}|r|1,\boldsymbol{q}\rangle\langle 1,\boldsymbol{q}|r|0,\boldsymbol{q}\rangle}{[E_{3,0}(\boldsymbol{q}) + \hbar\omega - i\gamma_{3,0}][E_{2,0}(\boldsymbol{q}) + 2\hbar\omega - i\gamma_{2,0}][E_{1,0}(\boldsymbol{q}) - \hbar\omega - i\gamma_{1,0}]} \\ & \left. + \frac{\langle 0,\boldsymbol{q}|r|3,\boldsymbol{q}\rangle\langle 3,\boldsymbol{q}|r|2,\boldsymbol{q}\rangle\langle 2,\boldsymbol{q}|r|1,\boldsymbol{q}\rangle\langle 1,\boldsymbol{q}|r|0,\boldsymbol{q}\rangle}{[E_{3,0}(\boldsymbol{q}) + \hbar\omega - i\gamma_{3,0}][E_{2,0}(\boldsymbol{q}) + 2\hbar\omega - i\gamma_{2,0}][E_{1,0}(\boldsymbol{q}) + 3\hbar\omega - i\gamma_{1,0}]} \right] d\boldsymbol{q}. \end{aligned} \tag{1}$$

Here, $\boldsymbol{q}$ denotes the electron wave vector from the K point, $|0\rangle$ is the initial state, $|i\rangle$ $(i = 1,\ 2,\ 3)$ is the ith excited state, $f_0[E_0(\boldsymbol{q}), E_F, T_e] = 1/(\exp\{[E_0(\boldsymbol{q}) - E_F]/k_B T_e\} + 1)$ is the Fermi-Dirac distribution factor for the state $|0, \boldsymbol{q}\rangle$ as a function of Fermi energy E_F and electron temperature T_e, $E_{i,0}$ is the energy difference between states $|0\rangle$ and $|i\rangle$, and $\gamma_{i,0}$ is the damping energy. Moreover, r is the electric-dipole operator, and the matrix element is given by $\langle c, \boldsymbol{q}|r|v, \boldsymbol{q}\rangle = -\frac{\hbar^2}{m\Delta E_{c,v}(\boldsymbol{q})}\langle c, \boldsymbol{q}|\nabla_r|v, \boldsymbol{q}\rangle = -\frac{\hbar^2}{m(2\hbar v_F|\boldsymbol{q}|)}\mathbf{M}^{cv}(\boldsymbol{q})$ and $\langle c, \boldsymbol{q}|r|c, \boldsymbol{q}\rangle = -\frac{\hbar^2}{m\Delta E_{c,c}(\boldsymbol{q})}\langle c, \boldsymbol{q}|\nabla_r|c, \boldsymbol{q}\rangle = -\frac{\hbar^2}{m(\hbar v_F\omega/c_0)}\mathbf{M}^{cc}(\boldsymbol{q})$ with the Fermi velocity $v_F = 10^6$ m/s [29] and speed of light in vacuum c_0. m is the mass of the electron, and $\Delta E_{a,b}(\boldsymbol{q}) = E_a(\boldsymbol{q}) - E_b(\boldsymbol{q})$ is the energy difference between states $|a\rangle$ and $|b\rangle$. The transition matrix element $\mathbf{M}^{ab}(\boldsymbol{q}) = \langle a, \boldsymbol{q}|\nabla_r|b, \boldsymbol{q}\rangle$ of graphene is obtained from the literature that adopts dipole approximation [30]. Since graphene has D_{6h} point-group symmetry, the following are the independent nonzero components: $\chi^{(3)}_{xxxx} = \chi^{(3)}_{yyyy} = \chi^{(3)}_{xxyy} + \chi^{(3)}_{xyxy} + \chi^{(3)}_{xyyx}$, $\chi^{(3)}_{xxyy} = \chi^{(3)}_{yyxx}$, $\chi^{(3)}_{xyxy} = \chi^{(3)}_{yxyx}$, and $\chi^{(3)}_{xyyy} = \chi^{(3)}_{yxxy}$ [18,21]. Under this condition, considering only $\chi^{(3)}_{xxxx}$ in the calculation is enough for simplicity.

To discuss the resonance effect in detail, we consider two THG processes using the π valence band (VB) and π^* conduction band (CB). The THG process within the third-order nonlinearity is a four-photon process comprising four transitions. The combination of interband and intraband transitions yields the combined process VB → CB → CB → CB → VB (including both intraband and interband transitions) and the interband process VB → CB → VB → CB → VB (comprising only interband transitions). Here, we exclude other processes, such as VB→VB→CB→VB→VB, VB→CB→CB→VB→VB,

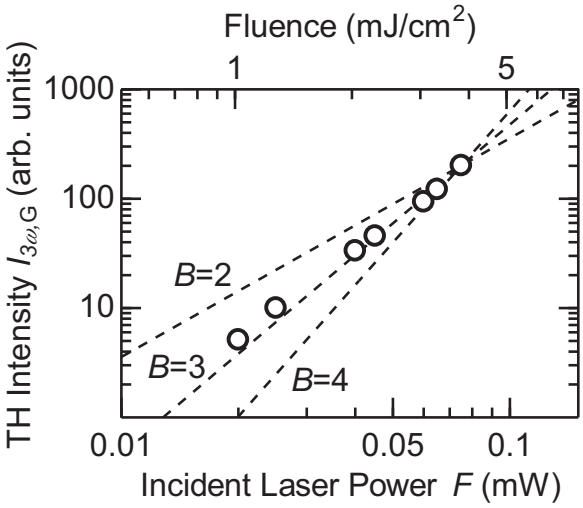

FIG. 3. Incident laser power dependence of the TH intensity of graphene. Circles represent the experimental results, and broken lines represent the slopes of 2, 3, and 4.

and VB→VB→CB→CB→VB. This is because the VB is filled with electrons, and intraband transitions within the VB do not actually contribute to THG. In the combined process, the electronic states of $|1\rangle$, $|2\rangle$, and $|3\rangle$ should belong to the CB, and the transition energies are $E_{3,0}(\boldsymbol{q}) = E_{2,0}(\boldsymbol{q}) = E_{1,0}(\boldsymbol{q}) = 2\hbar v_F|\boldsymbol{q}|$. However, in the interband process, $|1\rangle$ and $|3\rangle$ belong to the CB and $|2\rangle$ belongs to the VB. Here, transition energies are expressed as $E_{3,0}(\boldsymbol{q}) = E_{1,0}(\boldsymbol{q}) = 2\hbar v_F|\boldsymbol{q}|$ and $E_{2,0}(\boldsymbol{q}) = 0$. The damping energies of interband and intraband transitions are obtained from a previous study. These are described as $\gamma_{\text{inter}} = 0.2|E_F|$ [18,31] and $\gamma_{\text{intra}} = 0.5$ meV [18,32].

IV. RESULTS AND DISCUSSION

A. Photon energy dependence

First, we performed spectroscopic THG measurements of graphene on the SiO_2 substrate. Figures 2(a) and 2(b) present the intensity patterns of TH at 2066 nm for the SiO_2 substrate and as-grown graphene on the SiO_2 substrate, respectively, as functions of the incident angle (Maker fringe pattern). The intensity of graphene/SiO_2 is greater than that of SiO_2 due to the superposition of TH electric fields generated in graphene. Here, TH intensities of SiO_2 $I_{3\omega,S}$ and graphene $I_{3\omega,G}$ were extracted from the fringe patterns shown in Fig. 2. $I_{3\omega,S}$ is determined by the maximum intensity of the envelope of the fringe pattern for SiO_2 [broken line in Fig. 2(a)]. $I_{3\omega,G}$ is determined by the intensity of graphene/SiO_2 at the incident angle for which the intensity of SiO_2 is minimized [broken line in Fig. 2(b)].

Figure 3 presents the incident power dependence of $I_{3\omega,G}$. The experimental results for seven different power points exhibit a nonlinear increase in the TH intensity with the incident laser power. The broken lines in Fig. 3 represent the approximation curves for $I_{3\omega,G} = AF^B$. Here, A and B are the fitting parameters, and F is the incident laser power. The experimental results were fitted at $B = 2.79$, which is close to 3. Therefore, the observed signals are generated by third-order nonlinearity.

The spectrum of $\chi^{(3)} = |\chi^{(3)}|\exp(i\phi)$ of single-layer graphene was calculated by comparing the Maker fringe patterns of graphene/SiO_2 and SiO_2. The TH electric field generated from the SiO_2 substrate is given by $\tilde{E}_{3\omega,S} = \frac{E_{3\omega,S}}{2}[1 - \exp(-i\pi\frac{l}{l_{C,S}})]$ [33]. Here, l and $l_{C,S}$ are the optical path and coherent lengths of the SiO_2 substrate respectively. Specifically, $l_{C,S}$ is obtained by $l_{C,S} = \frac{\lambda}{6|n_{3\omega} - n_\omega|}$ as λ, n_ω, and $n_{3\omega}$ are the wavelength of incident laser light and the refractive indices at ω and 3ω (THG), respectively. The TH intensity of the fringe pattern from the SiO_2 substrate is given by

$$I_{3\omega,S} \propto |\tilde{E}_{3\omega,S}|^2 = \frac{E_{3\omega,S}^2}{2}\left[1 - \cos\left(\pi\frac{l}{l_{C,S}}\right)\right]. \tag{2}$$

Here, l is a function of incident angle θ and is given by $l = \frac{n_\omega d_S}{\sqrt{n_\omega^2 - \sin^2\theta}}$. From Eq. (2), $E_{3\omega,S}^2$ corresponds to the maximum intensity of the envelope of the fringe pattern for SiO_2 [broken line in Fig. 2(a)]. The complex TH electric field generated from the graphene film is given by $\tilde{E}_{3\omega,G} = iE_{3\omega,G}\exp(i\phi_G)$. Here, ϕ_G is the phase difference of $\tilde{E}_{3\omega,G}$ concerning $\tilde{E}_{3\omega,S}$. The TH intensity of the fringe pattern of graphene/SiO_2 is given by [34]

$$\begin{aligned} I_{3\omega,G+S} &\propto |\tilde{E}_{3\omega,G} + \tilde{E}_{3\omega,S}|^2 \\ &= E_{3\omega,G}^2 + \frac{E_{3\omega,S}^2}{2} - E_{3\omega,G}E_{3\omega,S}\sin\phi_G \\ &\quad + E_{3\omega,G}E_{3\omega,S}\cos\phi_G\sin\left(\pi\frac{l}{l_{C,S}}\right) \\ &\quad + \left(E_{3\omega,G}E_{3\omega,S}\sin\phi_G - \frac{E_{3\omega,S}^2}{2}\right)\cos\left(\pi\frac{l}{l_{C,S}}\right). \end{aligned} \tag{3}$$

By comparing the amplitude and incident angle for which the intensity is minimized in Eq. (3) with those of the experimental results, we can determine $E_{3\omega,G}/E_{3\omega,S}$ and ϕ_G [33,34]. $\chi_G^{(3)}$ was calculated by the following expression [33]:

$$\chi_G^{(3)} = \frac{2}{\pi}\frac{E_{3\omega,G}}{E_{3\omega,S}}\frac{\chi_S^{(3)}l_{C,S}}{d_G}\exp(i\phi_G), \tag{4}$$

where $\chi_S^{(3)}$ and d_G are the third-order NLO susceptibility of SiO_2 and the thickness of graphene ($d_G = 0.33$ nm [18]), respectively. The $|\chi_S^{(3)}|$ value was determined by applying the reported value (3.9×10^{-22} m^2/V^2 at 1907 nm [35]) to Miller's rule [36]. Moreover, as the phase of $\chi_S^{(3)}$ is zero [6], that of $\chi_G^{(3)}$ is identified as the phase difference of $\tilde{E}_{3\omega,G}$ concerning $\tilde{E}_{3\omega,S}$ (i.e., ϕ_G.) In a previous study on polysilanes, as $|\chi^{(3)}|$ and ϕ determined by the analysis of fringe patterns obey the Kramers-Kronig relationship [37], the validity of the method is satisfactorily assured.

The experimental spectra for the modulus $|\chi_G^{(3)}|$ and phase ϕ_G of complex third-order NLO susceptibility are presented in Fig. 4. Each value of $|\chi_G^{(3)}|$ and ϕ_G represents the average of the five experimental results. The $|\chi_G^{(3)}|$ values change from 7×10^{-10} to 2×10^{-10} esu with an increase in the photon energy from 0.57 to 0.81 eV. The modulus monotonically decreases with an increase in $\hbar\omega$. These values are comparable to those reported by Jiang *et al.* [18]. Additionally,

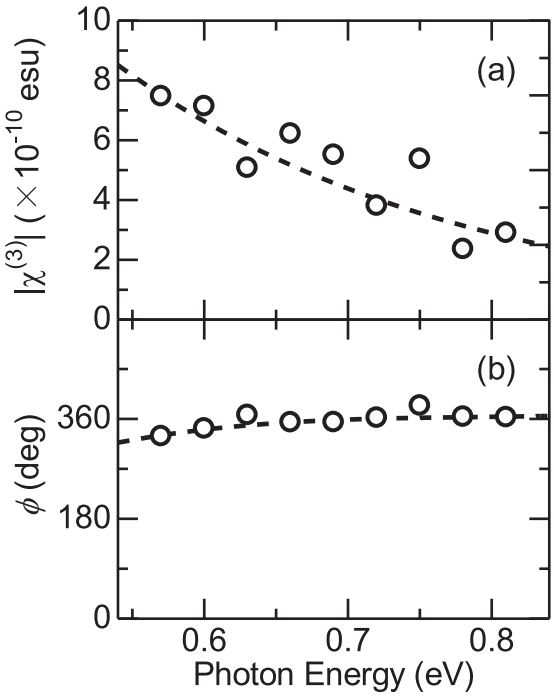

FIG. 4. Excitation photon energy dependence of the $\chi^{(3)}$ value of single-layer graphene. Circles represent the modulus (a) and the phase (b) of experimental results. Broken lines are guides for the eye.

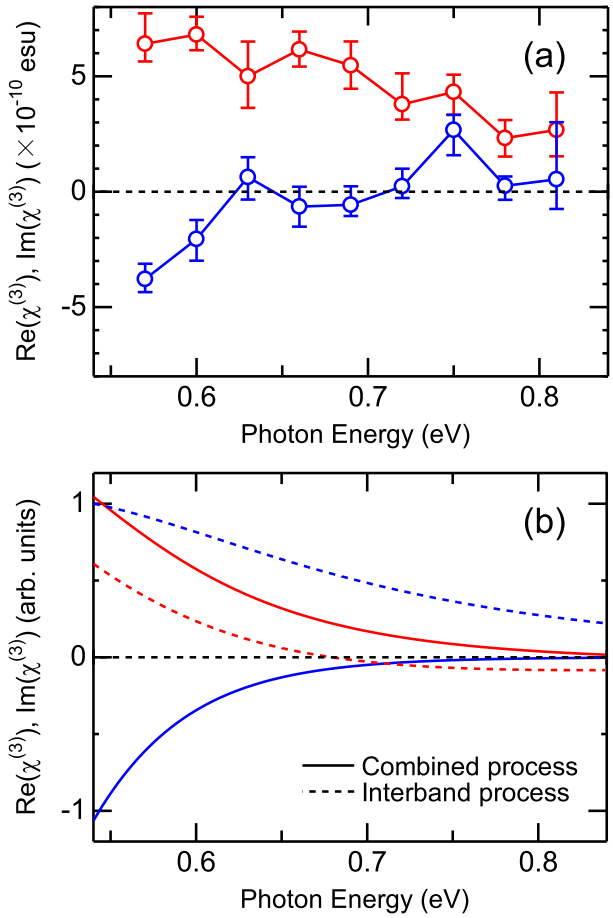

FIG. 5. (a) Real (red circles) and imaginary (blue circles) part spectra of the experimental $\chi^{(3)}$. (b) Real (red lines) and imaginary (blue lines) part spectra of the calculated $\chi^{(3)}$. Solid and broken lines are the calculated spectra based on the combined and interband processes, respectively.

ϕ_G gradually increases from 330 ° at 0.57 eV to 360 ° at 0.81 eV. These experimental phase values are consistent with the theoretical results reported by Margulis *et al.* [38]. Figure 5(a) shows the real and imaginary parts of $\chi^{(3)}$ converted from the experimentally obtained $|\chi_G^{(3)}|$ and ϕ_G spectrum. Here, $\chi_G^{(3)}$ has roughly the positive real and negative imaginary parts, and both approach zero with an increase in $\hbar\omega$.

Hereafter, we discuss the electronic processes contributing to THG in graphene. Figure 5(b) shows the calculated results of the $\chi^{(3)}$ spectrum using Eq. (1) at the electron temperature of 300 K. The moduli of $\chi^{(3)}$ of the combined process and interband process are normalized by absolute value $|\chi^{(3)}|$ at $\hbar\omega = 0.57$ eV. Both the $\chi^{(3)}$ spectra of the combined process and interband process show a monotonical decrease concerning $\hbar\omega$. When $E_{1,0}$, $E_{2,0}$, and $E_{3,0}$ are equal to either $\hbar\omega$, $2\hbar\omega$, or $3\hbar\omega$, $\chi^{(3)}$ exhibits a resonance effect. These resonances result from one-, two-, and three-photon resonances. $\chi^{(3)}$ includes the incident photon energy $\hbar\omega$ in the denominators of the integrand in Eq. (1). Therefore, as $\hbar\omega$ increases, the energy denominators of the integrand in Eq. (1) are increased, and $\chi^{(3)}$ monotonically decreases, which is consistent with the experimental result shown in Fig. 4(a). The calculated imaginary parts of $\chi^{(3)}$ for the combined and interband processes have different signs. In the combined process, the imaginary part of $\chi^{(3)}$ has negative values, and $\chi^{(3)}$ is located at the fourth quadrant in a complex plane. Meanwhile, the imaginary part of $\chi^{(3)}$ of the interband process has positive values, and $\chi^{(3)}$ is located at the first quadrant in a complex plane. From this difference of $\chi^{(3)}$, the present experimental result shows that the combined process dominates the THG process in graphene.

At each resonance energy, the imaginary component of the integrands in Eq. (1) exhibits a local maximum, and the real component is close to zero. As the products of the matrix elements $\langle 0|r|3\rangle\langle 3|r|2\rangle\langle 2|r|1\rangle\langle 1|r|0\rangle$ have positive real values, the dominant terms are all purely imaginary. To discuss resonant processes from the experimentally obtained $\chi_G^{(3)}$, we focus on the sign of the imaginary component of $\chi^{(3)}$ for each resonant process. We now discuss the denominator of Eq. (1). First, we consider the combined process at $\hbar\omega$. The first term on the integrands of Eq. (1), which is the dominant term of susceptibility, is determined by the product of the three energy denominators, that is, $(E_{1,0} - \hbar\omega - i\gamma)$, $(E_{2,0} - 2\hbar\omega - i\gamma)$, and $(E_{3,0} - 3\hbar\omega - i\gamma)$. The $\chi^{(3)}$ value is governed by the magnitudes of resonant denominators and those of nonresonant denominators. The magnitude of the nonresonant denominator is proportional to the energy difference between the one-/two-/three-photon energy and the energy difference between the relevant VB and CB states. The first denominator in Eq. (1), namely, $(E_{1,0} - \hbar\omega - i\gamma)$, is resonant when $\hbar\omega$ is equal to $E_{1,0}$ [Fig. 6(a)]. Hence, the second and third denominators in Eq. (1) are not resonant. The product of the two nonresonant denominators in the first term of Eq. (1) is $1/[(-\hbar\omega)(-2\hbar\omega)]$ for $\gamma \to 0$. When $E_{2,0}$ is equal to $2\hbar\omega$,

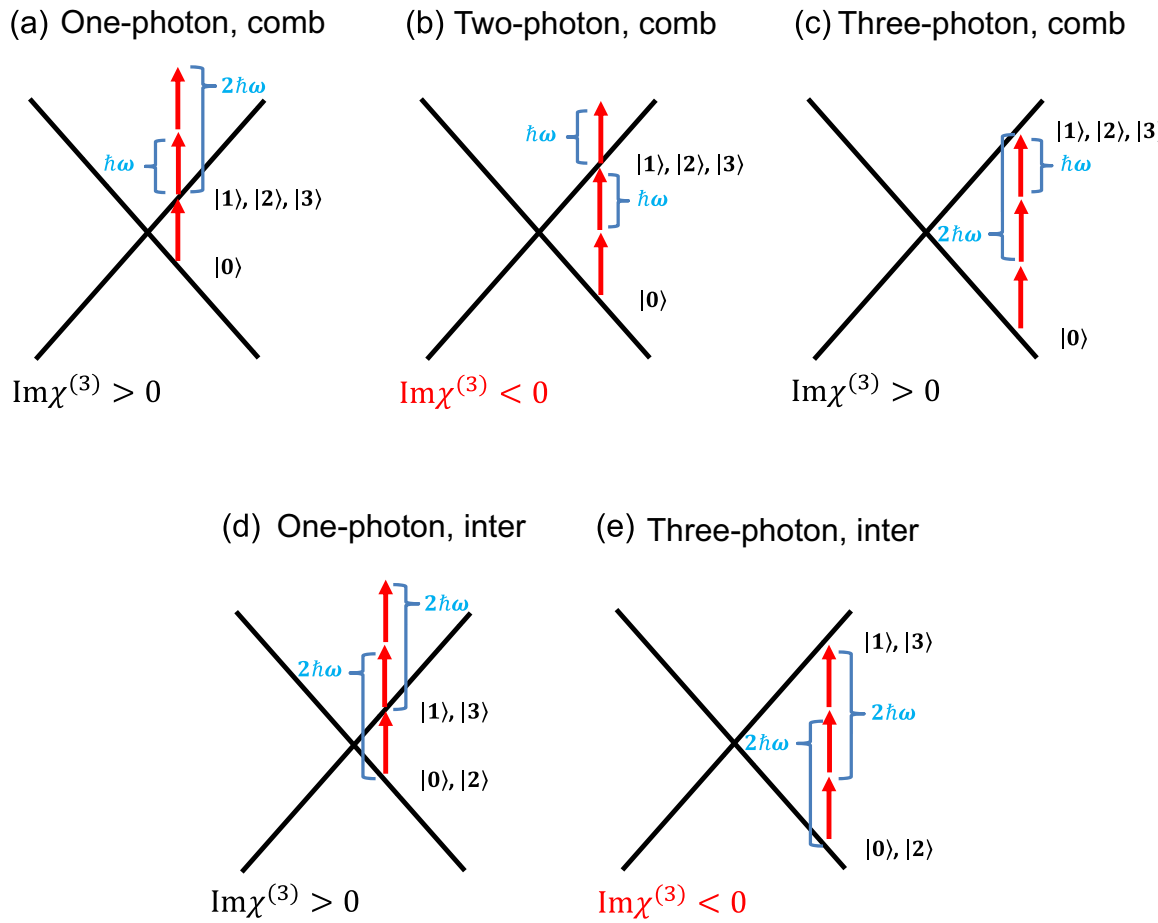

FIG. 6. Main resonance processes of THG in graphene. (a)–(c) One-, two-, and three-photon resonances of the combined process, and (d),(e) one- and three-photon resonances of the interband process corresponding to the first term in Eq. (1), respectively.

the first and third denominators are not resonant, and the product of the remaining two denominators in the first term of Eq. (1) is $1/[(\hbar\omega)(-\hbar\omega)]$ [Fig. 6(b)]. Similarly, considering that $E_{3,0} = 3\hbar\omega$ for the combined process [Fig. 6(c)], the product of the two nonresonant denominators in the first term of Eq. (1) is $1/[(2\hbar\omega)(\hbar\omega)]$. For the imaginary component of the combined model, the resonant components of the first term at $E_{1,0} = \hbar\omega$, $E_{2,0} = 2\hbar\omega$, and $E_{3,0} = 3\hbar\omega$ have a ratio of $1 : -2 : 1$. Similarly, if we calculate the resonance processes for all four terms in Eq. (1) and calculate the integral concerning $\boldsymbol{q}$, the ratio is $1 : -2 : 1$. Therefore, in Eq. (1), the one-photon resonance and three-photon resonance terms have the same sign and are constructive with each other, whereas that of the two-photon resonance has the opposite sign and is destructive to the one-photon and three-photon resonances. Therefore, when all three resonances operate, $\chi^{(3)}$ is expected to be suppressed.

In our experimental results, the phase is 330° (fourth quadrant in the complex $\chi^{(3)}$ plane) at $\hbar\omega = 0.57$ eV [Fig. 4(b)], and the imaginary component of $\chi^{(3)}$ has a negative value [Fig. 5(a)]. This experimental result indicates that two-photon resonance is the most significant in the THG process of the considered graphene in the Dirac electronic system [Fig. 6(b)]. This effective two-photon resonance is explained by the ratio of the energy denominators in Eq. (1). The more noticeable two-photon resonance at $\hbar\omega = 0.57$ eV compared to the other excitation energies can be understood as follows. When the E_F value of graphene is nonzero, electronic transitions with a transition energy of less than $2|E_F|$ are suppressed by Pauli blocking. The $2|E_F|$ value of the as-grown sample was estimated to be approximately 0.5 eV. When $\hbar\omega$ is equal to 0.57 eV, $\hbar\omega$ is relatively close to $2|E_F|(= 0.5$ eV) within the measurement range. Because the damping energy γ is $0.2|E_F|$ [31] and the electron temperature is 300 K, a portion of the contribution from the one-photon resonance of $\chi^{(3)}$ less than $2|E_F|$ is effectively restricted. Consequently, the cancellation of $\chi^{(3)}$ is weakened and the contribution from the two-photon resonance with a negative imaginary value is elicited. When $\hbar\omega$ increases to 0.81 eV, the two-photon resonance is canceled by the one-photon resonance because Pauli blocking does not occur, and $\chi^{(3)}$ is suppressed. Consequently, the $\chi^{(3)}$ value decreases from 7×10^{-10} to 2×10^{-10} esu as $\hbar\omega$ increases from 0.57 to 0.81 eV [Fig. 4(a)].

We also considered the contribution of the interband process to $\chi^{(3)}$ at a fixed $\hbar\omega$. $\chi^{(3)}$ exhibits a one-photon resonance and three-photon resonance when $E_{1,0}$ and $E_{3,0}$ are, respectively, equal to $\hbar\omega$ and $3\hbar\omega$ [Figs. 6(d) and 6(e)]. In such cases, the products of the two nonresonant denominators in the first term of Eq. (1) are $1/[(-2\hbar\omega)(-2\hbar\omega)]$ and $1/[(2\hbar\omega)(-2\hbar\omega)]$. For the imaginary component of the integral of the four terms in Eq. (1) for the interband model, considering the transition matrix elements, the ratio of the

resonant components at $E_{1,0} = \hbar\omega$ and $E_{3,0} = 3\hbar\omega$ is $1 : -\frac{1}{27}$. Equation (1) for the three-photon resonance has a small value compared to that for the one-photon resonance. Therefore, the imaginary part of $\chi^{(3)}$ is expected to be positive [Fig. 5(b)]. Because the dipole matrix elements of Eq. (1) for the combined process are greater than that for the interband process, the contribution of the interband process could be weak and was not observed in the experiment.

We compared our experimental results to those for other materials. For the THG process in graphene with $|E_F| = 0$, one-, two-, and three-photon resonances occur simultaneously, resulting in the self-cancellation of THG, whereas such simultaneous resonance does not occur in conventional insulating materials. In the latter case, a band gap exists and a clear resonant structure related to the optical gap can be observed [2,5,6]. For example, the $\chi^{(3)}$ spectra of polysilanes, which are known to be a typical one-dimensional insulator, exhibit three-photon resonance and two-photon resonance peaks corresponding to the excitonic states in the modulus spectra [6] when $3\hbar\omega$ and $2\hbar\omega$ are equal to the energies of the one-photon allowed excited state and one-photon forbidden state relative to the ground state, respectively. These behaviors contrast with those of graphene. $\chi^{(3)}$ of graphene remains in the fourth quadrant, suggesting that the two-photon resonance in the combined process dominates THG of graphene in a wide energy range. Therefore, this study demonstrates the peculiarity of the electronic states of graphene from the perspective of NLO responses.

B. Fermi energy dependence

To clarify the relationship between the resonance effects described above and Pauli blocking, we measured the E_F dependence of THG from graphene. Figure 7 shows the Maker fringe patterns of an ion-gel/graphene/ITO/ SiO_2 device at an excitation energy of 0.60 eV. The observed TH signal from the doping device contains four components of THG from an ion gel, graphene, ITO, and SiO_2. Here, as THG from an ion gel was too weak to be observed, we ignored the TH components from an ion gel in the following (see Supplemental Material, Fig. S2 [24]). To extract TH components from graphene, ITO, and SiO_2, we prepared bare areas of each layer on the device. Figure 7(a) shows the fringe pattern of SiO_2 observed where the SiO_2 surface is exposed (see embedded graphics). The black line in Fig. 7(b) shows the fringe pattern for the ITO/SiO_2 area. The amplitude of the fringe pattern of ITO/SiO_2 is larger than that of SiO_2. Additionally, the rotation angles at which the intensity was minimized were different between SiO_2 and ITO/SiO_2. This can be attributed to the interference of the TH electric fields generated in ITO and SiO_2. The red line in Fig. 7(b) shows the fringe pattern for the graphene/ITO/ SiO_2 zone. Further, the amplitude and period of the fringe pattern were different from that of ITO/SiO_2. Clearly, there is a contribution from the TH electric field generated in graphene. The TH signal from the graphene/ITO/ SiO_2 zone is explained by the superposition of TH electric fields generated in graphene, ITO, and SiO_2.

To extract the TH signal of graphene from the fringe pattern of graphene/ITO/ SiO_2, we analyzed the fringe patterns using the following method. The fringe pattern of TH intensity from the SiO_2 substrate is given by Eq. (2), as described

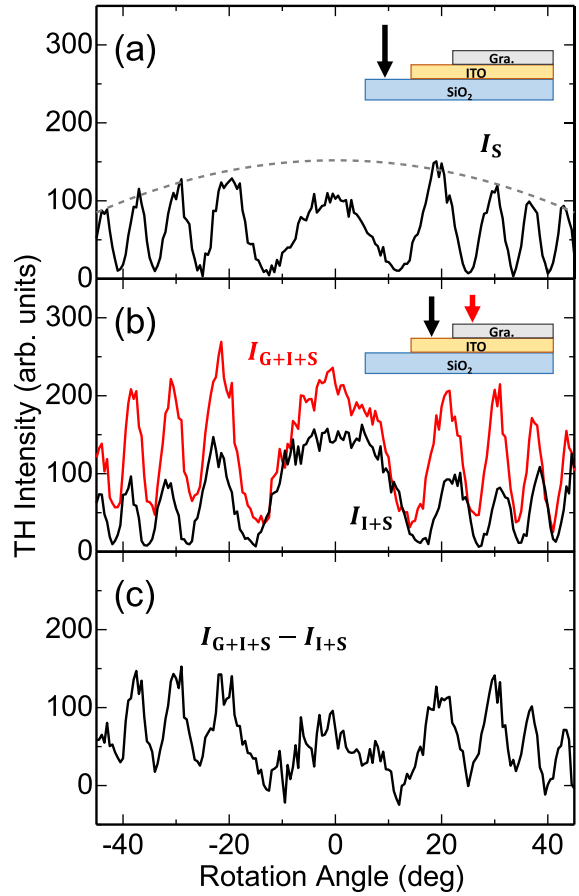

FIG. 7. Maker fringe patterns of the TH intensity as a function of the incident angle. (a) Black solid line shows a fringe pattern of the SiO_2 zone I_S, and broken line shows the envelope of the fringe pattern. (b) Black and red lines show the fringe patterns of ITO/SiO_2 I_{I+S} and graphene/ITO/SiO_2 I_{G+I+S}, respectively. (c) Difference of the fringe pattern between I_{G+I+S} and I_{I+S}.

in Sec. IV A. The complex TH electric field generated from a thin ITO film is given by $\tilde{E}_{3\omega,I} = iE_{3\omega,I}\exp(i\phi_I)$. Here, ϕ_I is the phase difference of $\tilde{E}_{3\omega,I}$ concerning $\tilde{E}_{3\omega,S}$. The TH intensity of the fringe pattern of ITO/SiO_2 is given by [34]

$$\begin{aligned} I_{3\omega,I+S} &\propto |\tilde{E}_{3\omega,I} + \tilde{E}_{3\omega,S}|^2 \\ &= E_{3\omega,I}^2 + \frac{E_{3\omega,S}^2}{2} - E_{3\omega,I}E_{3\omega,S}\sin\phi_I \\ &\quad + E_{3\omega,I}E_{3\omega,S}\cos\phi_I \sin\left(\pi\frac{l}{l_{C,S}}\right) \\ &\quad + \left(E_{3\omega,I}E_{3\omega,S}\sin\phi_I - \frac{E_{3\omega,S}^2}{2}\right)\cos\left(\pi\frac{l}{l_{C,S}}\right). \end{aligned} \quad (5)$$

From the analysis using Eq. (5), we obtained $E_{3\omega,I}/E_{3\omega,S}$ and ϕ_I (see Supplemental Material, Fig. S3 [24]). Here, the complex third-order nonlinear susceptibility of ITO $\chi^{(3)}_{ITO}$ varies by approximately 30% depending on applied voltage. In the Supplemental Material [24], we discussed $\chi^{(3)}_{ITO}$ and its doping concentration dependence. Additionally, the complex TH electric field generated from graphene is given

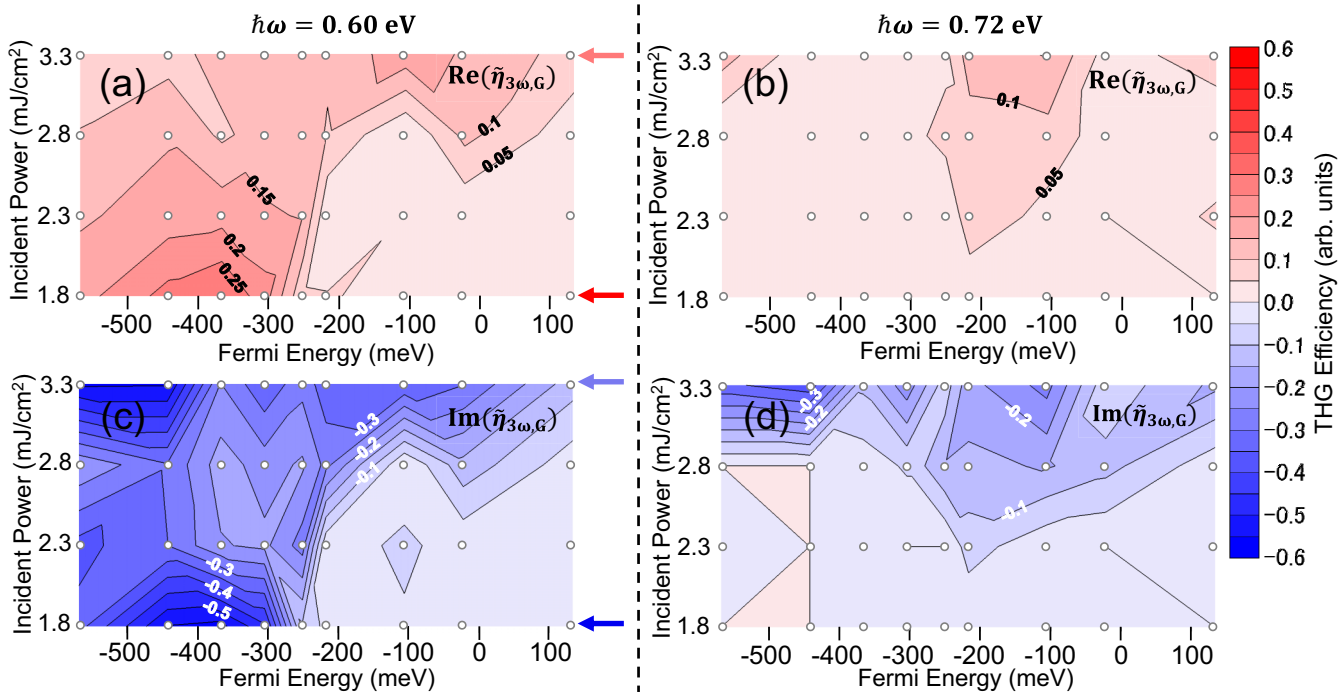

FIG. 8. Experimental THG efficiency $\tilde{\eta}_{3\omega,\mathrm{G}}$ with respect to the Fermi energy (x axis) and the incident laser power (y axis) for the real part of (a) 0.60 eV and (b) 0.72 eV and the imaginary part of (c) 0.60 eV and (d) 0.72 eV. White dots show the measurement points.

by $\tilde{E}_{3\omega,\mathrm{G}} = iE_{3\omega,\mathrm{G}}\exp(i\phi_{\mathrm{G}})$ as ϕ_{G} is the phase difference of $\tilde{E}_{3\omega,\mathrm{G}}$ concerning $\tilde{E}_{3\omega,\mathrm{S}}$. The TH intensity of fringe pattern of graphene/ITO/ SiO_2 is given by

$$\begin{aligned} I_{3\omega,\mathrm{G+I+S}} &\propto |\tilde{E}_{3\omega,\mathrm{G}} + \tilde{E}_{3\omega,\mathrm{I}} + \tilde{E}_{3\omega,\mathrm{S}}|^2 \\ &= E_{3\omega,\mathrm{G}}^2 + E_{3\omega,\mathrm{I}}^2 + \frac{E_{3\omega,\mathrm{S}}^2}{2} - E_{3\omega,\mathrm{G}}E_{3\omega,\mathrm{S}}\sin\phi_{\mathrm{G}} \\ &- E_{3\omega,\mathrm{I}}E_{3\omega,\mathrm{S}}\sin\phi_{\mathrm{I}} - 2E_{3\omega,\mathrm{G}}E_{3\omega,\mathrm{I}}\cos(\phi_{\mathrm{G}} + \phi_{\mathrm{I}}) \\ &+ (E_{3\omega,\mathrm{G}}E_{3\omega,\mathrm{S}}\cos\phi_{\mathrm{G}} + E_{3\omega,\mathrm{I}}E_{3\omega,\mathrm{S}}\cos\phi_{\mathrm{I}})\sin\left(\pi\frac{l}{l_{\mathrm{C,S}}}\right) \\ &+ \left(E_{3\omega,\mathrm{G}}E_{3\omega,\mathrm{S}}\sin\phi_{\mathrm{G}} + E_{3\omega,\mathrm{I}}E_{3\omega,\mathrm{S}}\sin\phi_{\mathrm{I}} - \frac{E_{3\omega,\mathrm{S}}^2}{2}\right) \\ &\times \cos\left(\pi\frac{l}{l_{\mathrm{C,S}}}\right). \end{aligned} \tag{6}$$

Subtracting Eq. (5) from Eq. (6), we obtained the following expression:

$$\begin{aligned} I_{3\omega,\mathrm{G+I+S}} - I_{3\omega,\mathrm{I+S}} &\propto E_{3\omega,\mathrm{G}}^2 - E_{3\omega,\mathrm{G}}E_{3\omega,\mathrm{S}}\sin\phi_{\mathrm{G}} \\ &- 2E_{3\omega,\mathrm{G}}E_{3\omega,\mathrm{I}}\cos(\phi_{\mathrm{G}} + \phi_{\mathrm{I}}) \\ &+ E_{3\omega,\mathrm{G}}E_{3\omega,\mathrm{S}}\sin\left(\pi\frac{l}{l_{\mathrm{C,S}}} + \phi_{\mathrm{G}}\right). \end{aligned} \tag{7}$$

The calculation result of $I_{3\omega,\mathrm{G+I+S}} - I_{3\omega,\mathrm{I+S}}$ is presented in Fig. 7(c). The analysis using Eq. (7) with the values of $E_{3\omega,\mathrm{I}}/E_{3\omega,\mathrm{S}}$ and ϕ_{I} obtained above provides $E_{3\omega,\mathrm{G}}/E_{3\omega,\mathrm{S}}$ and ϕ_{G}. Here, ϕ_{G} corresponds to the difference of the angle of the local minima in the Maker fringe pattern between $I_{3\omega,\mathrm{S}}$ and $I_{3\omega,\mathrm{G+I+S}} - I_{3\omega,\mathrm{I+S}}$.

We defined the complex THG efficiency of graphene as $\tilde{\eta}_{3\omega,\mathrm{G}} = \frac{E_{3\omega,\mathrm{G}}}{E_{3\omega,\mathrm{S}}}\exp(i\phi_{\mathrm{G}})$. Here, the TH electric field from SiO_2 is used as reference. In this experiment, we measured Maker fringe patterns for each Fermi energy and incident laser power. E_F was controlled from +133 to −568 meV by applying voltage to the electrodes. Incident laser power was fixed at 3.3, 2.8, 2.3, and 1.8 mJ/cm^2 per pulse using neutral density filters. The experimental fringe patterns were analyzed using Eqs. (5)–(7), and $E_{3\omega,\mathrm{G}}$ and ϕ_{G} were obtained. The complex $\tilde{\eta}_{3\omega,\mathrm{G}}$ converted from $E_{3\omega,\mathrm{G}}$ and ϕ_{G} are shown in Fig. 8. Here, the E_F dependence of $\tilde{\eta}_{3\omega,\mathrm{G}}$, which varies with the incident laser power, was observed. Figures 8(a)–8(d) show the real and imaginary parts of $\tilde{\eta}_{3\omega,\mathrm{G}}$ at 0.60 eV (0.72 eV) concerning E_F and the incident laser power. In Figs. 8(a)–8(d), the real and imaginary parts are positive and negative, respectively, regardless of E_F and the incident laser power. The magnitude of experimental $\tilde{\eta}_{3\omega,\mathrm{G}}$ at 0.60 eV is approximately twice as much as that at 0.72 eV. For the results at 0.60 eV, $\tilde{\eta}_{3\omega,\mathrm{G}}$ varies widely concerning E_F and the incident laser power. 1.8 mJ/cm^2 was strongly dependent on E_F and the magnitude of $\tilde{\eta}_{3\omega,\mathrm{G}}$.

To discuss the electronic processes of THG from these experimental results, we introduce the third-order nonlinear susceptibility $\chi^{(3)}$. Referring to Eq. (4), the susceptibility of graphene $\chi_{\mathrm{G}}^{(3)}$ is given from $\tilde{\eta}_{3\omega,\mathrm{G}}$ as

$$\chi_{\mathrm{G}}^{(3)} = \frac{2}{\pi}\frac{\chi_{\mathrm{S}}^{(3)}l_{\mathrm{C,S}}}{d_{\mathrm{G}}}\tilde{\eta}_{3\omega,\mathrm{G}}. \tag{8}$$

The values of $\chi_{\mathrm{G}}^{(3)}$ converted from the experimental $\tilde{\eta}_{3\omega,\mathrm{G}}$ using Eq. (8) are in 10^{-10} esu order of magnitude [right axis in Fig. 9(a)]. The absolute values of $\chi_{\mathrm{G}}^{(3)}$ are comparable to those reported in a previous study [18].

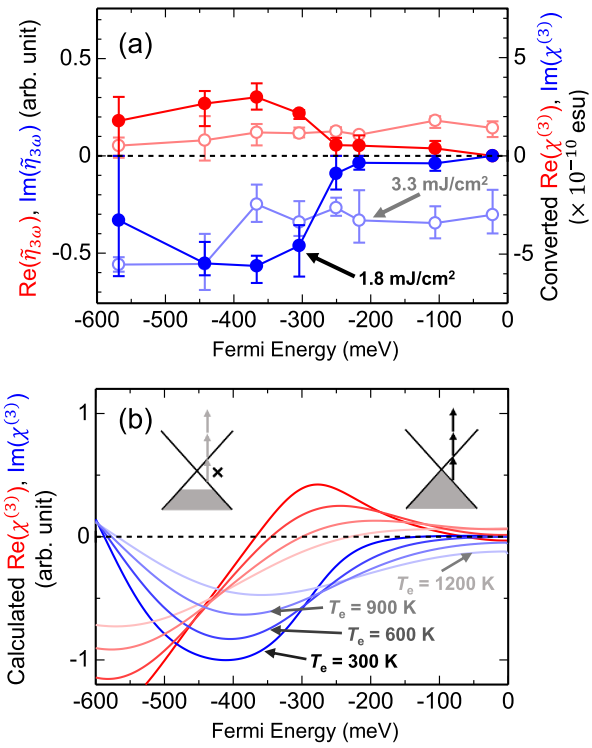

FIG. 9. (a) Experimental results of the THG efficiency $\tilde{\eta}_{3\omega,\mathrm{G}}$ for 3.3 mJ/cm^2 (open circles) and 1.8 mJ/cm^2 (filled circles) of 0.60 eV. The right axis shows the converted third-order nonlinear susceptibility $\chi^{(3)}_{\mathrm{G}}$ using Eq. (5). (b) Electron temperature dependence of the calculated spectra based on the combined process for $T_e = 300,\ 600,\ 900,$ and 1200 K.

Figure 9(b) shows the results of the model calculations of $\chi^{(3)}$ using Eq. (1) for the combined process. First, we considered resonance effects from the E_F dependence of the complex $\chi^{(3)}$. The model calculation at $T_e = 300$ K shows a peak structure in the real part and a steplike structure in the imaginary part at $E_F = -300$ meV. The drastic changes of $\chi^{(3)}$ are due to the restriction of one-photon resonance effects above $|E_F| = \hbar\omega/2$. In the combined model, while one-, two-, and three-photon resonances coexist, the one- and three-photon resonances cancel the two-photon resonance. Due to the restriction of one-photon resonance by Pauli blocking, the canceling relationship is relaxed, and $\chi^{(3)}$ is enhanced at $|E_F| = \hbar\omega/2$ [inset image in Fig. 9(b)]. The change of $\chi^{(3)}$ at $|E_F| = \hbar\omega/2$ in this model calculation coincides with our experimental result in Fig. 9(a) and clarifies the restriction effect of one-photon resonance in our experiments.

Second, we focus on the laser power dependence of THG. The laser power dependence is explained by an increase in T_e [18–20], which is induced by one-photon absorption at $\hbar\omega > 2|E_F|$. When the laser pulse is irradiated to graphene, the electrons in the VB are excited to the CB. The generated photocarriers are relaxed through electron-electron interaction in a few tens of femtoseconds, and the hot electrons are thermalized [39]. Consequently, the photoabsorption contributes to an increase in T_e within the pulse time width of 100 fs [40]. In the calculation model described above, we considered T_e in $f_0[E_0(\boldsymbol{q}), E_F, T_e]$. When T_e increases, the $\boldsymbol{q}$ dependence of the distribution function of initial states $f_0[E_0(\boldsymbol{q}), E_F, T_e]$ becomes gradual, and $\chi^{(3)}$ changes. When the linear absorption α_0 is 2.3%, the peak intensity of the incident pulse I is 33 GW/cm^2, the theoretical saturation intensity I_S is 0.07 GW/cm^2 [41], and the optical absorption α $[= \alpha_0/(1 + I/I_S)]$ is about 4.87×10^{-3} (%). At $E_F = -250$ meV, the electronic specific heat is $C_e = 1.4 \times 10^{-9} T_e$ (J/m^2 K) [42]. T_e $(= T_0 + \alpha F/C_e$ [20]) is estimated as ∼1200 K for $F = 3.3$ mJ/cm^2. Here, we assumed that T_e increases to 1200 K by photoabsorption and calculated $\chi^{(3)}$. Figure 9(b) shows the T_e dependence of the calculated $\chi^{(3)}$. As T_e is increased from 300 to 1200 K, the peak structure of the real part and the steplike structure of the imaginary part around $E_F = -300$ meV are smoothed. This smoothing reproduces the behaviors in the experimental results of -400 meV $< E_F$ for an increase in the laser power from 1.8 to 3.3 mJ/cm^2 [Fig. 9(a)]. In the energy range of $0 < |E_F| < \hbar\omega/2$, smoothing of the distribution function at high T_e reduces the one-photon resonant $\chi^{(3)}$ component, leading to the reduction of the cancellation of two-photon resonance. Consequently, the absolute value of Im $\chi^{(3)}$ at 1200 K becomes larger than that at 300 K. Moreover, the calculated Im($\chi^{(3)}$) of 1200 K approaches zero with a decrease in $|E_F|$, while the experimental Im($\chi^{(3)}$) of 3.3 mJ/cm^2 deviates from zero. The difference is explained by the change of T_e concerning E_F. Because C_e is proportional to $|E_F|$, T_e increases as the $|E_F|$ decreases even for the constant laser power [42]. In the range of $0 < |E_F| < \hbar\omega/2$, the calculated |Im $\chi^{(3)}$| decreases in response to a decrease in $|E_F|$ [Fig. 9(b)]. Owing to these competing factors, the experimental Im($\chi^{(3)}$) of 3.3 mJ/cm^2 would be constant concerning $|E_F|$. Focusing on the range of $\hbar\omega/2 < |E_F|$, the experimental results of the imaginary part at $E_F \sim -443$ and -568 meV do not match the calculated results. For these Fermi energies, the experimental results of the imaginary part for 1.8 and 3.3 mJ/cm^2 have close values. This behavior shows that T_e is not significantly affected depending on excitation density at $E_F \sim -443$ and -568 meV. The reason for this behavior is because the electron temperature is not increased due to the restriction of the one-photon absorption by Pauli blocking at $\hbar\omega/2 < |E_F|$.

We explained the laser power dependence of the THG efficiency $\tilde{\eta}_{3\omega,\mathrm{G}}$ by converting $\tilde{\eta}_{3\omega,\mathrm{G}}$ to third-order susceptibility $\chi^{(3)}$ in the above paragraph. Generally, the susceptibility $\chi^{(3)}$ is the proportional coefficient of the third-order nonlinear polarization to the incident electric field E^3_ω. It should also have no laser power dependence within the third-order nonlinearity. However, our experimental results confirmed that the laser power dependence of $\chi^{(3)}$ is non-negligible. Therefore, we considered the possibility of other contributions, such as THGs due to the fifth-order nonlinear susceptibility $\chi^{(5)}(-3\omega; \omega, -\omega, \omega, \omega, \omega)$. However, this explanation is denied by the fact that the fifth-harmonic generation (FHG) $\chi^{(5)}(-5\omega, \omega, \omega, \omega, \omega, \omega)$ is not observed in our experiment (see Supplemental Material, Fig. S4 [24]). THG and FHG in the fifth-order nonlinear process should use the common electronic states; the transition matrix elements involved in $\chi^{(5)}(-3\omega; \omega, -\omega, \omega, \omega, \omega)$ and $\chi^{(5)}(-5\omega; \omega, \omega, \omega, \omega, \omega)$ are common. Therefore, the contribution of THG due to $\chi^{(5)}$ is negligible because FHG is not observed. Therefore, the

above-mentioned explanation of the laser power dependence of THG is based on third-order nonlinearity and implies the importance of effects of increased T_e in $\chi^{(3)}$. Recently, high-harmonic generation (HHG) based on not perturbative, but nonperturbative, treatment has been considerably discussed. Such nonperturbative theories mainly stem from the experimental observation of the breakdown of the power law. Meanwhile, our above-mentioned experimental results of the laser power dependence of complex $\chi^{(3)}$ propose that an increase in T_e can break the power law in THG. This indicates that the HHG experiments using a high-power laser pulse of a few TW/cm^2 [12] could induce an increase in T_e, which should be considered on the basis of perturbative treatment.

Finally, we discussed the differences in real parts of $\chi^{(3)}$ between the experimental results of Fig. 9(a) and the calculated results of Fig. 9(b). In the experimental result, $\mathrm{Re}\chi^{(3)}$ has positive values regardless of E_F in the region of $|E_F| \leqslant 568$ meV. Conversely, the sign of $\mathrm{Re}\chi^{(3)}$ changes from positive to negative with doping in the calculated result. Here, as one possible reason for this difference, we propose a contribution from nonresonant $\chi^{(3)}$. In our calculation, the contribution from the nonlinear region of band dispersion beyond 3.2 eV is not included. In a previous study on absorption spectra, graphene showed strong absorption by the transition at the M point above 4.5 eV [43]. The strong absorption is due to the Van Hove singularity of density of states at the M point. Similarly, in the THG process, the TH intensity enhancement by three-photon resonance at the M point was reported [15]. The overall $\mathrm{Re}(\chi^{(3)})$ comprises resonant $\chi^{(3)}$ using the band of linear dispersion and nonresonant $\chi^{(3)}$ related to the Van Hove singularity at the M point. Assuming the combined process at the M point, $\mathrm{Re}(\chi^{(3)})$ and $\mathrm{Im}(\chi^{(3)})$ have positive values at $\hbar\omega = 0.60$ eV from the first term of Eq. (1). Under a nonresonant condition below the transition energy of the M point, the decrease of the energy denominator of $[E-3\hbar\omega-i\gamma]^{-1}$ concerning $\hbar\omega$ is milder for the real part than for the imaginary part. This ensures that the contribution of the real part is larger than that of the imaginary part at $\hbar\omega = 0.60$ eV. Consequently, the nonresonant contribution is added to $\mathrm{Re}(\chi^{(3)})$, and the sign of experimental $\mathrm{Re}(\chi^{(3)})$ has positive values regardless of E_F. This finding could be the basis for understanding the resonance process of other third-order nonlinearity in graphene, such as two-photon absorption [44], optical Kerr effect [45–47], four-wave mixing [18,48,49], and NLO waveguide [50]. Additionally, these insights provide fundamental information to understand third-order nonlinear responses in other three-dimensional Dirac materials, such as Bi_2Se_3 [51] and TaAs [52].

V. CONCLUSION

We measured the complex third-order nonlinear susceptibility $\chi^{(3)}$ of as-grown single-layer graphene using the Maker fringe method. The modulus of $\chi^{(3)}$ exhibits a monotonic decrease with an increase in $\hbar\omega$ from 0.57 to 0.81 eV, and its values change from 7×10^{-10} to 2×10^{-10} esu. The $\chi^{(3)}$ phase gradually increases from 330 ° to 360 ° in the corresponding energy range. These phase values were discussed based on three dominant resonance processes. Through model calculation, we revealed that two-photon resonance is the most significant in THG of graphene. Furthermore, using the ion-gel-gated graphene device, we investigated the E_F dependence of THG and obtained $\chi^{(3)}$, converted from the TH efficiency as a function of E_F. For both the real and imaginary parts of $\chi^{(3)}$, their absolute values increase without changes in the sign around $|E_F| = \hbar\omega/2$. As E_F shifts from -106 to -568 meV, the $\chi^{(3)}$ modulus changes from 5.4×10^{-11} to 6.4×10^{-10} esu. This behavior clarifies that the one-photon resonance effect by Pauli blocking is suppressed and that two-photon resonance dominates THG in graphene. Moreover, we observed a smoothing of the E_F dependence of $\chi^{(3)}$ with increasing incident laser power. The laser power dependence is explained by the effect of the increase in electron temperature due to one-photon absorption. Moreover, we proposed the presence of a contribution of nonresonant $\chi^{(3)}$ using the Van Hove singularity at the M point from the comparison between experimental and calculated results. The presented results suggest the importance of resonance effects in revealing harmonic generation mechanisms in graphene. $\chi^{(3)}$ depending on $\hbar\omega$ and E_F indicates that the phase rotates clockwise in a complex plane as $2|E_F|/\hbar\omega$ increases (see Supplemental Material, Fig. S5 [24]). Therefore, the resonance process in graphene is dominated by Pauli blocking of $2|E_F|$. A study of resonance effects in lowest-order nonlinear processes, such as THG, can provide crucial information regarding higher-order NLO responses in novel electronic materials.

ACKNOWLEDGMENTS

This study was supported by the DII Collaborative Graduate Program for Accelerating Innovation in Future Electronics at Nagoya University; JST SPRING Grant No. JPMJSP2125, JST CREST Grant No. JPMJCR1901; and JSPS KAKENHI Grants No. JP17H02764, No. JP21H05232, No. JP21H05233, No. JP21K18878, and No. JP18H03864.

[1] P. N. Butcher and D. Cotter, *The Elements of Nonlinear Optics* (Cambridge University Press, New York, 1990).

[2] B. J. Orr and J. F. Ward, Perturbation theory of the non-linear optical polarization of an isolated system, Mol. Phys. **20**, 513 (1971).

[3] W. Leupacher and A. Penzkofer, Third-order nonlinear susceptibilities of dye solutions determined by third-harmonic generation, Appl. Phys. B **36**, 25 (1985).

[4] W. E. Torruellas, D. Neher, R. Zanoni, G. I. Stegeman, F. Kajzar, and M. Leclerc, Dispersion measurements of the third-order nonlinear susceptibility of polythiophene thin films, Chem. Phys. Lett. **175**, 11 (1990).

[5] D. A. Akimov, M. V. Alfimov, S. O. Konorov, A. A. Ivanov, S. Botti, A. A. Podshivalov, R. Ciardi, L. De Dominicis, L. S. Asilyan, R. Fantoni, and A. M. Zheltikov, Second- and third-harmonic generation by carbon nanotubes irradiated

with femtosecond laser pulses, J. Exp. Theor. Phys. **98**, 220 (2004).

[6] T. Hasegawa, Y. Iwasa, H. Sunamura, T. Koda, Y. Tokura, H. Tachibana, M. Matsumoto, and S. Abe, Nonlinear Optical Spectroscopy on One-Dimensional Excitons in Silicon Polymer, Polysilane, Phys Rev. Lett. **69**, 668 (1992).

[7] H. Kishida, M. Ono, K. Miura, H. Okamoto, M. Izumi, T. Manako, M. Kawasaki, Y. Taguchi, Y. Tokura, T. Tohyama, K. Tsutsui, and S. Maekawa, Large Third-Order Optical Nonlinearity of Cu-O Chains Investigated by Third-Harmonic Generation Spectroscopy, Phys. Rev. Lett. **87**, 177401 (2001).

[8] R. Wang, H.-C. Chien, J. Kumar, N. Kumar, H.-Y. Chiu, and H. Zhao, Third-harmonic generation in ultrathin films of MoS_2, ACS Appl. Mater. Interfaces **6**, 314 (2014).

[9] S. Ghimire, A. D. DiChiara, E. Sistrunk, P. Agostini, L. F. DiMauro, and D. A. Reis, Observation of high-order harmonic generation in a bulk crystal, Nat. Phys. **7**, 138 (2010).

[10] M. Hohenleutner, F. Langer, O. Schubert, M. Knorr, U. Huttner, S. W. Koch, M. Kira, and R. Huber, Real-time observation of interfering crystal electrons in high-harmonic generation, Nature (London) **523**, 572 (2015).

[11] H. Liu, Y. Li, Y. S. You, S. Ghimire, T. F. Heinz, and D. A. Reis, High-harmonic generation from an atomically thin semiconductor, Nat. Phys. **13**, 262 (2017).

[12] N. Yoshikawa, T. Tamaya, and K. Tanaka, High-harmonic generation in graphene enhanced by elliptically polarized light excitation, Science **356**, 736 (2017).

[13] S. Kovalev, R. M. A. Dantas, S. Germanskiy, J.-C. Deinert, B. Green, I. Ilyakov, N. Awari, M. Chen, M. Bawatna, J. Ling, F. Xiu, P. H. M. van Loosdrecht, P. Surówka, T. Oka, and Z. Wang, Non-perturbative terahertz high-harmonic generation in the three-dimensional Dirac semimetal Cd_3As_2, Nat. Commun. **11**, 2451 (2020).

[14] N. Kumar, J. Kumar, C. Gerstenkorn, R. Wang, H.-Y. Chiu, A. L. Smirl, and H. Zhao, Third harmonic generation in graphene and few-layer graphite films, Phys. Rev. B **87**, 121406(R) (2013).

[15] S.-Y. Hong, J. I. Dadap, N. Petrone, P.-C. Yeh, J. Hone, and R. M. Osgood, Jr., Optical Third-Harmonic Generation in Graphene, Phys. Rev. X **3**, 021014 (2013).

[16] A. Säynätjoki, L. Karvonen, J. Riikonen, W. Kim, S. Mehravar, R. A. Norwood, N. Peyghambarian, H. Lipsanen, and K. Kieu, Rapid large-area multiphoton microscopy for characterization of graphene, ACS Nano **7**, 8441 (2013).

[17] R. I. Woodward, R. T. Murray, C. F. Phelan, R. E. P. de Oliveira, T. H. Runcorn, E. J. R. Kelleher, S. Li, E. C. de Oliveira, G. J. M. Fechine, G. Eda, and C. J. S. de Matos, Characterization of the second- and third-order nonlinear optical susceptibilities of monolayer MoS_2 using multiphoton microscopy, 2D Mater. **4**, 011006 (2017).

[18] T. Jiang, D. Huang, J. Cheng, X. Fan, Z. Zhang, Y. Shan, Y. Yi, Y. Dai, L. Shi, K. Liu, C. Zeng, J. Zi, J. E. Sipe, Y.-R. Shen, W.-T. Liu, and S. Wu, Gate-tunable third-order nonlinear optical response of massless Dirac fermions in graphene, Nat. Photonics **12**, 430 (2018).

[19] G. Soavi, G. Wang, H. Rostami, D. G. Purdie, D. D. Fazio, T. Ma, B. Luo, J. Wang, A. K. Ott, D. Yoon, S. A. Bourelle, J. E. Muench, I. Goykhman, S. D. Conte, M. Celebrano, A. Tomadin, M. Polini, G. Cerullo, and A. C. Ferrari, Broadband, electrically tunable third-harmonic generation in graphene, Nat. Nanotechnol. **13**, 583 (2018).

[20] G. Soavi, G. Wang, H. Rostami, A. Tomadin, O. Balci, I. Paradisanos, E. A. A. Pogna, G. Cerullo, E. Lidorikis, M. Polini, and A. C. Ferrari, Hot electrons modulation of third-harmonic generation in graphene, ACS Photonics. **6**, 2841 (2019).

[21] J. L. Cheng, N. Vermeulen, and J. E. Sipe, Third order optical nonlinearity of graphene, New J. Phys. **16**, 053014 (2014).

[22] H. Ago, K. Kawahara, Y. Ogawa, S. Tanoue, M. A. Bissett, M. Tsuji, H. Sakaguchi, R. J. Koch, F. Fromm, and T. Seyller, Epitaxial growth and electronic properties of large hexagonal graphene domains on Cu(111) thin film, Appl. Phys. Express **6**, 075101 (2013).

[23] P. D. Maker, R. W. Terhune, M. Nisenoff, and C. M. Savage, Effects of Dispersion and Focusing on the Production of Optical Harmonics, Phys. Rev. Lett. **8**, 21 (1962).

[24] See Supplemental Material at http://link.aps.org/supplemental/10.1103/PhysRevB.108.075408 for additional experimental details and analysis.

[25] D. Inukai, T. Koyama, M. Araidai, K. Kawahara, K. Ago, and H. Kishida, Fermi energy dependence of ultrafast photoluminescence from graphene, J. Appl. Phys. **132**, 134301 (2022).

[26] C.-F. Chen, C.-H. Park, B. W. Boudouris, J. Horng, B. Geng, C. Girit, A. Zettl, M. F. Crommie, R. A. Segalman, S. G. Louie, and F. Wang, Controlling inelastic light scattering quantum pathways in graphene, Nature (London) **471**, 617 (2011).

[27] J. E. Lee, G. Ahn, J. Shim, Y. S. Lee, and S. Ryu, Optical separation of mechanical strain from charge doping in graphene, Nat. Commun. **3**, 1024 (2012).

[28] A. Das, S. Pisana, B. Chakraborty, S. Piscanec, S. K. Saha, U. V. Waghmare, K. S. Novoselov, H. R. Krishnamurthy, A. K. Geim, and A. C. Ferrari, Monitoring dopants by Raman scattering in an electrochemically top-gated graphene transistor, Nat. Nanotechnol. **3**, 210 (2008).

[29] M. S. Dresselhaus and G. Dresselhaus, Intercalation compounds of graphite, Adv. Phys. **51**, 1 (2002).

[30] E. Malic, T. Winzer, E. Bobkin, and A. Knorr, Microscopic theory of absorption and ultrafast many-particle kinetics in graphene, Phys. Rev. B **84**, 205406 (2011).

[31] S. D. Sarma, S. Adam, E. H. Hwang, and E. Rossi, Electronic transport in two-dimensional graphene, Rev. Mod. Phys. **83**, 407 (2011).

[32] J. L. Cheng, N. Vermeulen, and J. E. Sipe, Third-order nonlinearity of graphene: Effects of phenomenological relaxation and finite temperature, Phys. Rev. B **91**, 235320 (2015).

[33] K. Kubodera and H. Kobayashi, Determination of third-order nonlinear optical susceptibilities for organic materials by third harmonic generation, Mol. Cryst. Liq. Cryst. **182**, 103 (1990).

[34] T. Hasegawa, Y. Iwasa, T. Koda, H. Kishida, Y. Tokura, S. Wada, H. Tashiro, H. Tachibana, M. Matsumoto, and R. D. Miller, Nonlinear optical study of polysilanes, J. Phys. Soc. Jpn. **63**(Suppl. B), 64 (1994).

[35] F. Kajzar and J. Messier, Third-harmonic generation in liquids, Phys. Rev. A **32**, 2352 (1985).

[36] R. C. Miller, Optical second harmonic generation in piezoelectric crystals, Appl. Phys. Lett. **5**, 17 (1964).

[37] H. Kishida, T. Hasegawa, Y. Iwasa, T. Koda, and Y. Tokura, Dispersion Relation in the Third-Order Electric Susceptibility for Polysilane Film, Phys. Rev. Lett. **70**, 3724 (1993).

[38] V. A. Margulis, E. E. Muryumin, and E. A. Gaiduk, Frequency dependence of optical third-harmonic generation from doped graphene, Phys. Lett. A **380**, 304 (2016).

[39] D. Brida, A. Tomadin, C. Manzoni, Y. J. Kim, A. Lombardo, S. Milana, R. R. Nair, K. S. Novoselov, A. C. Ferrari, G. Cerullo, and M. Polini, Ultrafast collinear scattering and carrier multiplication in graphene, Nat. Commun. **4**, 1987 (2013).

[40] P. B. Allen, Theory of Thermal Relaxation of Electrons in Metals, Phys. Rev. Lett. **59**, 1460 (1987).

[41] A. Marini, J. D. Cox, and F. J. García de Abajo, Theory of graphene saturable absorption, Phys. Rev. B **95**, 125408 (2017).

[42] D. Sun, C. Divin, C. Berger, W. A. de Heer, P. N. First, and T. B. Norris, Hot carrier cooling by acoustic phonons in epitaxial graphene by ultrafast pump-probe spectroscopy, Phys. Status Solidi C **8**, 1194 (2011).

[43] K. F. Mak, L. Ju, F. Wang, and T. F. Heinz, Optical spectroscopy of graphene: From the far infrared to the ultraviolet, Solid State Commun. **152**, 1341 (2012).

[44] H. Yang, X. Feng, Q. Wang, H. Huang, W. Chen, A. T. S. Wee, and W. Ji, Giant two-photon absorption in bilayer graphene, Nano Lett. **11**, 2622 (2011).

[45] H. Zhang, S. Virally, Q. Bao, L. K. Ping, S. Massar, N. Godbut, and P. Kockaert, *Z*-scan measurement of the nonlinear refractive index of graphene, Opt. Lett. **37**, 1856 (2012).

[46] E. Dremetsika, B. Dlubak, S.-P. Gorza, C. Ciret, M.-B. Martin, S. Hofmann, P. Seneor, D. Dolfi, S. Massar, P. Emplit, and P. Kockaert, Measuring the nonlinear refractive index of graphene using the optical Kerr effect method, Opt. Lett. **41**, 3281 (2016).

[47] N. Vermeulen, D. Castelló-Lurbe, J. Cheng, I. Pasternak, A. Krajewska, T. Ciuk, W. Strupinski, H. Thienpont, and J. V. Erps, Negative Kerr Nonlinearity of Graphene as Seen via Chirped-Pulse-Pumped Self-Phase Modulation, Phys. Rev. Appl. **6**, 044006 (2016).

[48] E. Hendry, P. J. Hale, J. Moger, A. K. Savchenko, and S. A. Mikhailov, Coherent Nonlinear Optical Response of Graphene, Phys. Rev. Lett. **105**, 097401 (2010).

[49] R. Ciesielski, A. Comin, M. Handloser, K. Donkers, G. Piredda, A. Lombardo, A. C. Ferrari, and A. Hartschuh, Graphene near-degenerate four-wave mixing for phase characterization of broadband pulses in ultrafast microscopy, Nano Lett. **15**, 4968 (2015).

[50] K. Alexander, N. A. Savostianova, S. A. Mikhailov, B. Kuyken, and D. V. Thourhout, Electrically tunable optical nonlinearities in graphene-covered SiN waveguides characterized by four-wave mixing, ACS Photonics **4**, 3039 (2017).

[51] F. Giorgianni, E. Chiadroni, A. Rovere, M. Cestelli-Guidi, A. Perucchi, M. Bellaveglia, M. Castellano, D. D. Giovenale, G. D. Pirro, M. Ferrario, R. Pompili, C. Vaccarezza, F. Villa, A. Cianchi, A. Mostacci, M. Petrarca, M. Brahlek, N. Koirala, S. Oh, and S. Lupi, Strong nonlinear terahertz response induced by Dirac surface states in Bi_2Se_3 topological insulator, Nat. Commun. **7**, 11421 (2016).

[52] L. Wu, S. Patankar, T. Morimoto, N. L. Nair, E. Thewalt, A. Little, J. G. Analytis, J. E. Moore, and J. Orenstein, Giant anisotropic nonlinear optical response in transition metal monopnictide Weyl semimetals, Nat. Phys. **13**, 350 (2016).